PLANE-WAVE LEAST-SQUARE REVERSE TIME MIGRATION WITH ENCODING STRATEGIES

CHUANG LI[1], JIANPING HUANG[1,3], ZHENCHUN LI[1] and RONGRONG WANG[2]

[1] *Department of Geophysics, School of Geosciences, China University of Petroleum, Qingdao 266580, P.R. China. jphuang@mail.ustc.edu.cn*
[2] *College of Information and Control Engineering, China university of Petroleum, Qingdao 266580, P.R.China.*
[3] *Earth Science Department, Rice University, Houston, TX 77005, U.S.A.*

(Received January 16, 2015; revised version accepted January 15, 2016)

ABSTRACT

Li, C., Huang, J., Li, Z. and Wang, R., 2016. Plane-wave least-square reverse time migration with encoding strategies. *Journal of Seismic Exploration*, 25: 177-197.

Plane-wave Least-Squares Reverse Time Migration (PLSRTM) delivers high resolution images with less computational cost compared with conventional Least-Squares Reverse Time Migration (LSRTM). But a great number of computational cost is still necessary to suppress migration artefacts. The study of plane-wave encoding strategy with better migration artefacts reduction may help to further improve the computational efficiency. In this paper, we present the theory and work flow of PLSRTM method; furthermore four different encoding strategies are applied to PLSRTM including static encoding, dynamic encoding, hybrid encoding and random dynamic encoding. Additionally, the illumination preconditioner and the mixed optimization method are introduced to accelerate the convergence rate. The numerical tests are implemented both on the synthetic data of Marmousi model and the 2D field data to compare the image quality and the computational cost of different encoding strategies. The results suggest that the static encoding method has a best imaging quality but highest computational cost while the improved encoding strategies have better computational efficiency which is suitable for the processing of mass data. Among them, PLSRTM with hybrid encoding has the advantage of less I/O cost and PLSRTM with random dynamic encoding shows better imaging quality and convergence with less iteration.

KEY WORDS: least-square migration, plane-wave encoding, encoding strategy, randomized sampling.

0963-0651/16/$5.00

INTRODUCTION

With increasing complexity of exploration targets, it is difficult for traditional acquisition to explore the complex area effectively. Thus, more and more high-density seismic acquisition methods with small surface element and high coverage times are used recently. Due to the enormous data of high-density acquisition, the method for encoding large number of common shots to several supergathers is provided to improve efficiency (Berkhout, 1992). However, the migration results will be blurred by the limited frequency band and the acquisition geometry because of directly regarding the adjoint instead of the inverse of modelling as the migration operator (Claerbout, 1992). Under the inversion framework, the gradient-based optimization schemes can be applied to the migration method to solve this problem in data domain.

Areal shot migration is firstly proposed (Berkhout, 1992) to encode the shot data to produce one supergather and achieves improved migration efficiency, and then the plane-wave migration is implemented in common offset domain by Radon transform (Mosher et al., 1997). Because the plane waves are produced by stacking a set of linear time-shifting gathers which are coherent signals, the migration image of one plane-wave does not contain crosstalk noise. However, the migration of plane-waves introduces aliasing artifacts (Dai et al., 2013) which degrades the quality of final images. Thus, the approach based on stacking the images from several plane-waves with different shooting angles is proposed to suppress migration artifacts and produce high-resolution images of complex structures (Chen et al., 2002; Liu et al., 2002; Zhang et al., 2005). However, conventional plane-wave migration still has its problem of low signal-to-noise ratio (SNR) and resolution in dealing with unconventional reservoirs. By involving the imaging problem into the inversion framework, the imaging results can be significantly improved with local optimization method (Tarantola, 1984; 1987). Lambaré et al. (1992) propose the linearized prestack inversion of seismic profiles based on the classical optimization theory. The linearized inversion are also implemented to invert the perturbations of P- and S-wave impedances and density in the elastic media (Jin et al., 1992). After that, the Least-Square Migration (LSM) is implemented on Kirchhoff migration operator to suppress the recording footprint noise due to the coarse receiver interval (Nemeth et al., 1999). LSM can deliver high resolution and amplitude-preserved images with huge computational cost (Dai et al., 2011; 2012; Huang et al., 2014). To combine the advantages of plane-wave migration and LSM, Dai et al. (2013) firstly introduce plane-wave encoding to Least-Square Reverse Time Migration(LSRTM) and testify the encoding strategies of dynamic encoding to further improve computational efficiency. Li et al. (2014a) apply the improved Plane-wave Least-Square Reverse Time Migration (PLSRTM) method to the imaging of fault block reservoirs. Wang et al. (2014) extend the 2D plane-wave least-squares Kirchhoff migration to 3D. Additionally, Li et al. (2014b) present the PLSRTM method for rugged

topography with modified plane-wave encoding function to avoid datum correction. For the previous studies, the implementation of plane-wave encoding strategies are mainly static encoding and dynamic encoding approaches. But a considerable amount of computation is still necessary to implement the static encoding approach, while the dynamic encoding approaches are penalized by huge I/O cost. Thus some improved encoding strategies should be proposed and discussed with other encoding approaches for better practical application.

In this paper, we present the PLSRTM method with four different encoding strategies including static encoding, dynamic encoding, hybrid encoding and random dynamic encoding. To improve imaging quality and accelerate the convergence rate, we also introduce the illumination preconditioner and the mixed optimization operator into the PLSRTM method. After that, the new imaging method is applied to the synthetic data of Marmousi model and field data set to evaluate the imaging quality, amplitude preservation ability, convergence rate, computational and I/O cost of PLSRTM with different encoding strategies.

METHODS

Plane-wave encoding method of observed data

For a two-dimensional exploration area, encoding process of shot records can be expressed as,

$$U(x;x_p,\omega) = \int u(x;x_s,\omega)e^{i\omega p x_s}\, dx_s \quad , \qquad (1)$$

where $u(x;x_s,\omega)$ denotes the observed common receiver record which is generated from the source at the location of x_s and recorded by geophones at x, and $U(x;x_p,\omega)$ is the encoded plane-wave from a synthesized line source at x_p. From eq. (1), the common-receiver gathers are transformed into a single trace from a line-source wavefield, which is equivalent to producing plane-waves by the tau-p transform method, which also can be physically interpreted as the delay shot acquisition. In the time domain, $e^{i\omega p x_s}$ refers to a time-shift which changes linearly with source location, while p denotes the ray parameter with the expression $p = \sin\theta/v$. Here θ is the incident angle at the surface, and v is the near-surface velocity. The schematic diagram of plane-wave encoding is modified from Zhang's method shown in Fig. 1 (Zhang et al., 2005).

Born modelling in plane-wave domain

In the plane-wave domain, the solution of the Helmholtz equation can be expressed as,

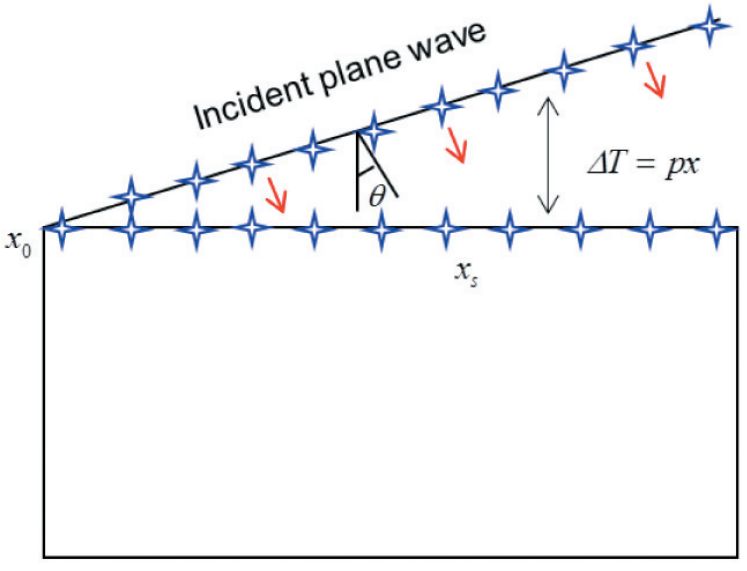

Fig. 1. Diagram of plane-wave encoding modified from Zhang's method (Zhang et al., 2005).

$$U_0(x;x_p) = W(\omega)G_0(x;x_p) \quad , \tag{2}$$

where $G_0(x;x_p)$ is the Green's function corresponding to background slowness s_o, $U_0(x;x_p)$ denotes the wavefield related to the plane-wave source at the location of x_p, and $W(\omega)$ denotes the wavelet of the synthesized line source which is set as a series of point sources.

We assume the background slowness perturbation is $\delta s(x)$, thus the true slowness model can be described as $s(x) = s_o + \delta s(x)$. The wavefield $U(x;x_p)$ from source to the imaging point underground can be obtained by solving the Helmholtz equation with slowness model $s(x)$:

$$[\nabla^2 + \omega^2 s(x)^2]U(x;x_p) = F \quad , \tag{3}$$

where the item $F = -\delta(x - x_p)W(\omega)$ represents the plane-wave source. Then substituting $s(x) = s_o + \delta s(x)$ into eq. (3) we can get:

$$[\nabla^2 + \omega^2 s_0^2 + 2\omega^2 s_0 \delta s(x)]U(x;x_p) = F \quad , \tag{4}$$

where the high-order term $O(\delta s^2)$ is neglected because of the small background slowness perturbation.

After that, we transform the third term of eq. (4) to the right side, and both sides are multiplied with Green's function $G_0(x;x')$, then integrate over the

whole volume with index x′. According to the Helmholtz equation of background wavefield $[\nabla^2 + \omega^2 s_0(x)^2]U_0(x;x_p) = -\delta(x - x')W(\omega)$ and eq. (2), we can find out the following equation $[\nabla^2 + \omega^2 s_0^2]p)G_0(x;x') = -\delta(x - x')$. Finally, the left hand side (LHS) and right hand side (RHS) of eq. (4) can be rewritten as,

$$\begin{aligned}
\text{LHS} &= \int [\nabla^2 + \omega^2 s_0^2]p)G_0(x;x')U(x';x_p)dx' \\
&= -\int U(x';x_p)\delta(x - x')dx' = U(x;x_p) \quad , \\
\text{RHS} &= \int G_0(x;x')Fdx' - 2\omega^2 \int s_0\delta s(x')U(x';x_p)G_0(x;x')dx' \\
&= -\int G_0(x;x')\delta(x - x')W(\omega)dx' \\
&\quad + \omega^2 \int m(x')W(\omega)G(x';x_p)G_0(x;x')dx' \\
&= U_0(x;x_p) + \omega^2 \int m(x')W(\omega)G(x';x_p)G_0(x;x')dx' \quad , \qquad (5)
\end{aligned}$$

where $m(x') = -2s_0\delta s(x')$ is defined as the reflectivity. Assuming slowness perturbation is small enough and applying the Born approximation $G(x';x_p) \approx G_0(x';x_p)$ to the RHS equation, we can calculate the scattered field as:

$$\begin{aligned}
U_1(x;x_p) &= U(x;x_p) - U_0(x;x_p) \\
&= \omega^2 \int m(x')W(\omega)G(x';x_p)G_0(x;x')dx' \\
&\approx \omega^2 \int m(x')W(\omega)G_0(x';x_p)G_0(x;x')dx' \quad . \qquad (6)
\end{aligned}$$

Thus the reverse time migration operator (Baysal et al., 1983) in the plane wave domain is

$$m_{mig}(x) = \sum_{x_p} \int \omega^2 W^*(\omega)U_1(x';x_p)G_0^*(x;x_p)G_0^*(x';x)dx' \quad . \qquad (7)$$

where * means the adjoint of the matrix, $m_{mig}(x)$ denotes the migration results which is the stacked images of different plane-waves at x_p.

To simplify the formula, Born modeling operator and plane-wave reverse time migration are presented by a vector matrix notation, respectively,

$$\mathbf{d} = \mathbf{Lm} \; ; \; \mathbf{m} = \mathbf{L}^T\mathbf{d} \quad , \qquad (8)$$

where **m** is the matrix form of migration profile or reflectivity model; **d** is the matrix form of plane-wave records; **L** and $\mathbf{L}^T$ denote Born modelling and reverse time migration in plane-wave domain, respectively.

Preconditioning operator

In our method, an illumination operator (Beydoun and Mendes, 1989; Luo and Schuster, 1991) is applied as the preconditioning into the gradient to compensate the weak illumination of deep area. The operator can be expressed as,

$$I(x) = \sum_{x_p} \int \omega^4 \mathrm{Re}\{G(x;x_p,\alpha)G^*(x;x_p,\omega)\}d\omega \quad , \tag{9}$$

where I(x) is the illumination operator in plane-wave domain which is calculated by stacking the illumination energy from different plane-waves at x_p and Re{ } denotes the real part of the operator. Additionally, a high-pass filter is applied to the gradient as the preconditioning at the first 3 iterations which can decrease the low frequency noise in the migration results.

Plane-wave least-squares reverse time migration

For one plane-wave records of ray parameter p, the misfit function in plane-wave domain can be expressed as,

$$f_1(\mathbf{m}) = \tfrac{1}{2} \| \mathbf{L}_p\mathbf{m}_p - \mathbf{d}_p \|^2 \quad , \tag{10}$$

where $\mathbf{L}_p$, $\mathbf{m}_p$ and $\mathbf{d}_p$, and are Born modelling, migration operator and observed data corresponding to the plane-wave with ray parameter p, respectively.

In this paper, a preconditioned conjugate gradient method is used to solve the misfit function in plane-wave domain,

$$\begin{aligned}
&\mathbf{g}^{(k+1)} = \mathbf{L}_p^T[\mathbf{L}_p\mathbf{m}_p^{(k)} - \mathbf{d}_p] \quad , \\
&\beta^{(k)} = (\mathbf{g}^{(k+1)}\mathbf{I}\mathbf{g}^{(k+1)})/(\mathbf{g}^{(k)}\mathbf{I}\mathbf{g}^{(k)}) \quad , \\
&\mathbf{z}^{(k+1)} = \mathbf{I}\mathbf{g}^{(k+1)} + \beta^{(k)}\mathbf{z}^{(k)} \quad , \\
&\alpha^{(k+1)} = ([\mathbf{z}^{(k+1)}]^T\mathbf{g}^{(k+1)})/([\mathbf{L}_p\mathbf{z}^{(k+1)}]^T\mathbf{L}_p\mathbf{z}^{(k+1)}) \quad , \\
&\mathbf{m}_p^{(k+1)} = \mathbf{m}_p^{(k)} - \alpha^{(k+1)}\mathbf{z}^{(k+1)} \quad ,
\end{aligned} \tag{11}$$

where k is the iteration number; $\mathbf{g}^{(k+1)}$, $\mathbf{z}^{(k+1)}$, $\alpha^{(k+1)}$ are steepest descent gradient, the conjugate gradient and the update step length at iteration number $k+1$, respectively. $\mathbf{I}$ is the illumination preconditioning operator which is discussed in the previous section.

However, only one plane-wave record is not enough to illuminate all the underground structures and suppress strong migration artefacts. High-quality images can be obtained by stacking images from the plane-wave records with different shooting angles. Assuming there are N plane-waves, the misfit function of prestack PLSRTM can be modified as,

$$f_2(\mathbf{m}) = \tfrac{1}{2} \sum_{i=1}^{N} \| \mathbf{L}_i \mathbf{m}_i - \mathbf{d}_i \|^2 = \tfrac{1}{2} \| \tilde{\mathbf{L}} \tilde{\mathbf{m}} - \tilde{\mathbf{d}} \|^2 , \tag{12}$$

$$\tilde{\mathbf{L}} = \begin{pmatrix} \mathbf{L}_1 & & & \\ & \mathbf{L}_2 & & \\ & & \ddots & \\ & & & \mathbf{L}_N \end{pmatrix}, \quad \tilde{\mathbf{m}} = \begin{pmatrix} \mathbf{m}_1 \\ \mathbf{m}_2 \\ \\ \\ \mathbf{m}_N \end{pmatrix} .$$

where $\mathbf{d}_i$ denotes the i-th plane-wave gather, $\mathbf{L}_i$ and $\mathbf{m}_i$ are Born modeling operator and migration image related to the i-th plane-wave, respectively; $\tilde{\mathbf{L}}$, $\tilde{\mathbf{m}}$, $\tilde{\mathbf{d}}$ denote Born modeling operator, the prestack image and the plane-waves, respectively. Thus the misfit is given as the summation of the data residual of plane-waves, and the migration images of different plane-waves are updated independently. The optimization is also implemented with the preconditioned conjugate gradient method to solve the misfit function (12).

In general, the optimization can be converged after n iterations ideally when the objective function is n-dimensional quadratic differentiable function. However, the inversion is usually failed to converge after n iterations due to the existence of ambient noise, calculation errors and other instability factors (Chen et al., 1985). Thus the conjugate gradient method implemented in this paper will recalculate the steepest descent direction and restart the algorithm after every five iterations. The workflow diagram of the new PLSRTM is shown in Fig. 2.

Encoding strategies

Generally, there are several encoding strategies. The PLSRTM mentioned above do not change the computed plane-waves at each iteration which is called

static encoding. Prestack PLSRTM with static encoding can suppress migration artefacts by stacking images of plane-waves with different ray parameters, but large amount of calculation is necessary. In order to further improve computational efficiency, Schuster et al. (2011), Dai et al. (2013) have proposed a dynamic encoding approach. The misfit of this approach can be given as,

$$f_3(\mathbf{m}) = \tfrac{1}{2} \left\| \mathbf{L}_{s(t)}\mathbf{m} - \mathbf{d}_{s(t)} \right\|^2 , \tag{13}$$

where s(i) is a sampling function which represents a label corresponding to the ray parameter of plane-waves. The relation between the label s(i) and the ray parameter is $p = p_{min} + s(i)\Delta p$, where Δp here means the interval of p in each

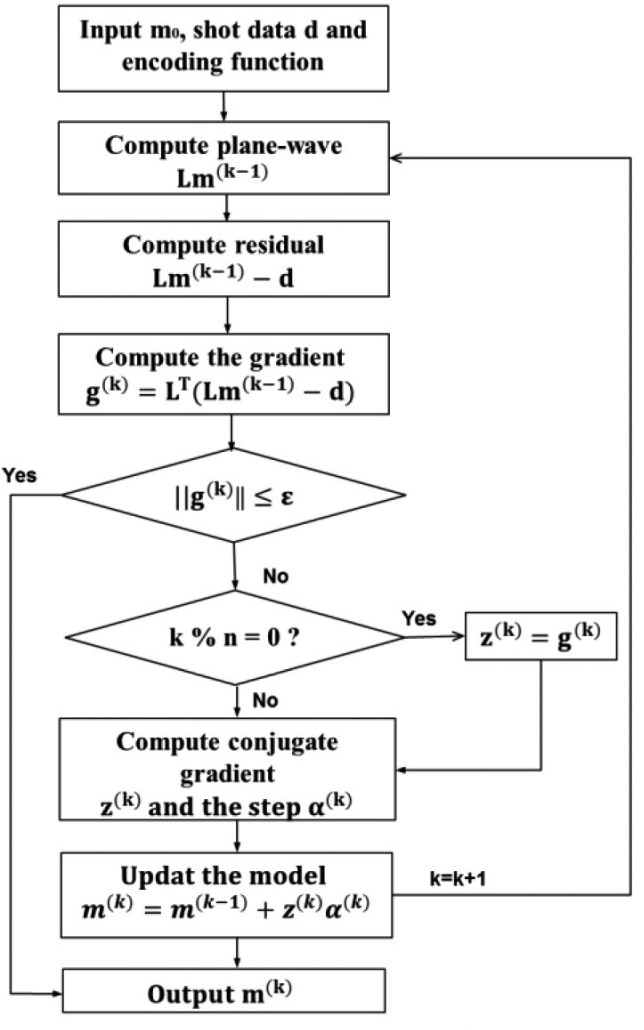

Fig. 2. Flow chart of PLSRTM.

iteration and p_{min} is the minimum value of p. The value of s(i) varies with i (iterations) uniformly in the dynamic approach just like Fig. 3b shows. In this approach, niter (maximum number of iterations) plane-wave records are encoded, which results in huge I/O cost.

Thus this paper introduces hybrid encoding strategy into PLSRTM, in which the value of changes one time with every n (n is chosen manually) iterations. Only niter/n plane-waves are generated, so the I/O cost is only 1/n times of the dynamic approach. Ray parameters of plane-wave records for each iterations of hybrid encoding are plotted in Fig. 3c, and here we set n equals 5.

In the two strategies we mentioned above, the plane-waves are chosen in a defined sequence for each iteration. Since the angles of plane-waves are defined uniformly, structures with some specific angles cannot be fully illuminated by only a few iterations. So we propose the randomized sampling approach to the dynamic encoding strategy, in which the value of s(i) is selected randomly for each iteration as shown in Fig. 3d. Although there are no computational improvements, randomized sampling allows more information for the original iterations which result in faster convergence and better images of complex structures.

In a word, the misfit of all the three strategies with single plane-waves can be expressed by eq. (13), but the value of s(i) is different. For example, eqs. (10) and (13) will be equivalent if s(i) is a constant which represents the plane-wave with ray parameter p. The preconditioned conjugate gradient method is implemented to find out the solution of the misfit as eq. (13) shows.

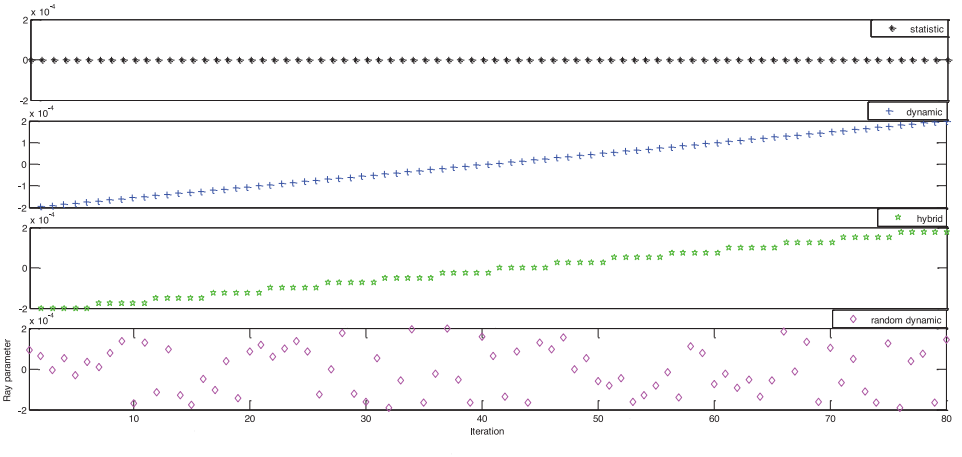

Fig. 3. Ray parameter of computed plane-waves for each iteration.

EXAMPLES

PLSRTM with static encoding

In this section, the PLSRTM with different encoding strategies are applied to the synthetic data set of Marmousi model. The size of the velocity model is 7.57 × 3.5 km with a 10 m grid interval. The inversion starts with the migration velocity model which is smoothed by the true velocity using the median filter method (Fig. 4a). Firstly, we calculate a perturbation model as the slowness difference $\delta s_{true} = s^2_{true} - s^2_0$ between the real model and the smoothed model (Fig. 4b).

Then shot-domain data are generated with fixed spread geometry where 757 shots are distributed with a 10 m shot interval. Each shot is recorded by 757 receivers with a 10 m receiver interval. A Ricker wavelet with a 30 Hz peak frequency is used as the source wavelet, and the record length is 3 s in time with a 0.5 ms interval. After the simulation, all the shot gathers are processed to get rid of the direct wave and surface wave. To implement the PLSRTM, 757 shot gathers are encoded to generate 24 plane-wave gathers with the shooting angles range from −30 to +30 degrees. Fig. 5 shows the encoded plane-wave records with different ray parameters. As the velocity model has complicated structures and strong lateral velocity variations, the reflection events of plane-waves are very intricate. To begin with, the shot data are implemented with conventional reverse time migration(RTM) for comparison, and the Laplace filtering image is shown in Fig. 6. Although RTM can produce clear image of most subsurface structures, the profiles contain obvious migration noise. In addition, the steep structures in the middle part can not be imaged correctly.

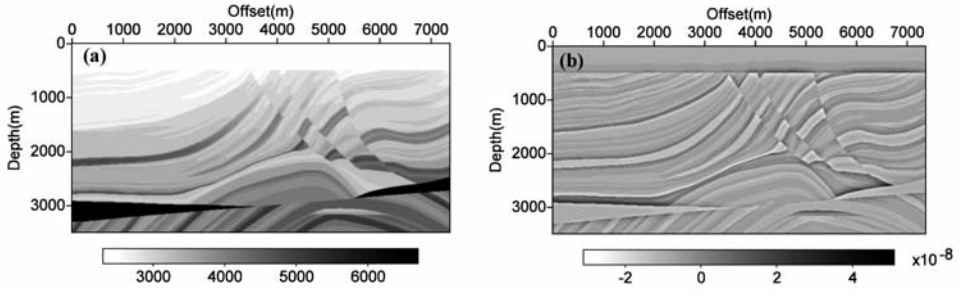

Fig. 4. Marmousi model. (a) real velocity; (b) real reflectivity.

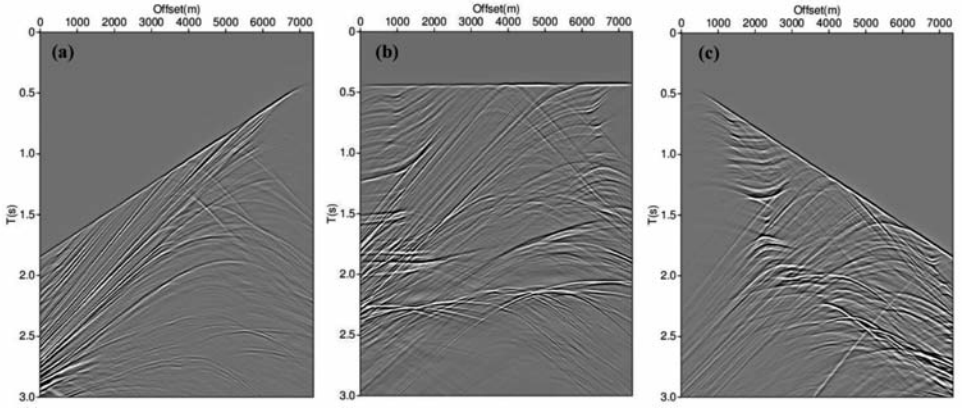

Fig. 5. Plane-wave records with (a) p = −0.5 ms/m; (b) p = 0 ms/m; (c) p = 0.5 ms/m.

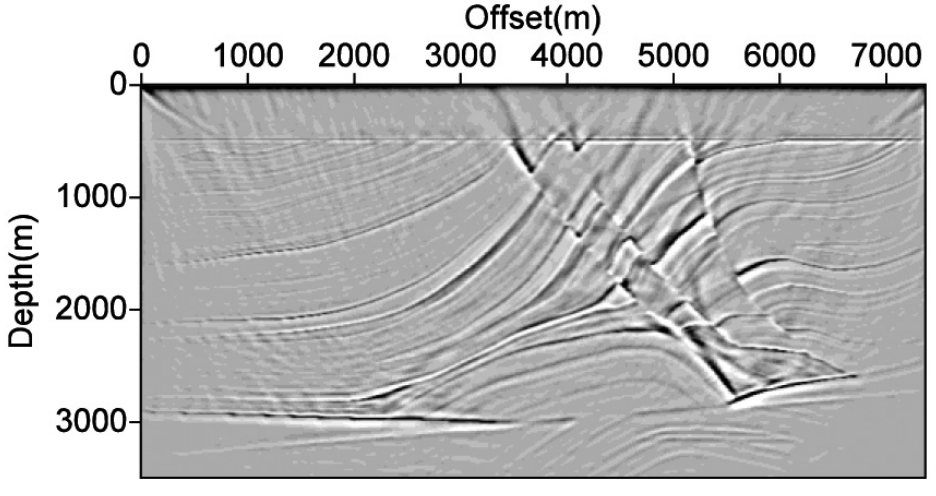

Fig. 6. Image of the traditional RTM.

After that, PLSRTM is applied to a single plane-wave record with a ray parameter of 0.0 ms/m and 0.5 ms/m, respectively, and the results are shown in Fig. 7. We can see that the image of only one plane-wave record contains strong artefacts which cannot be completely suppressed by optimization. Besides, the plane-wave source has obvious direction illumination characteristics, and the image is of highest resolution when incident angle of plane-wave is perpendicular to the target structure.

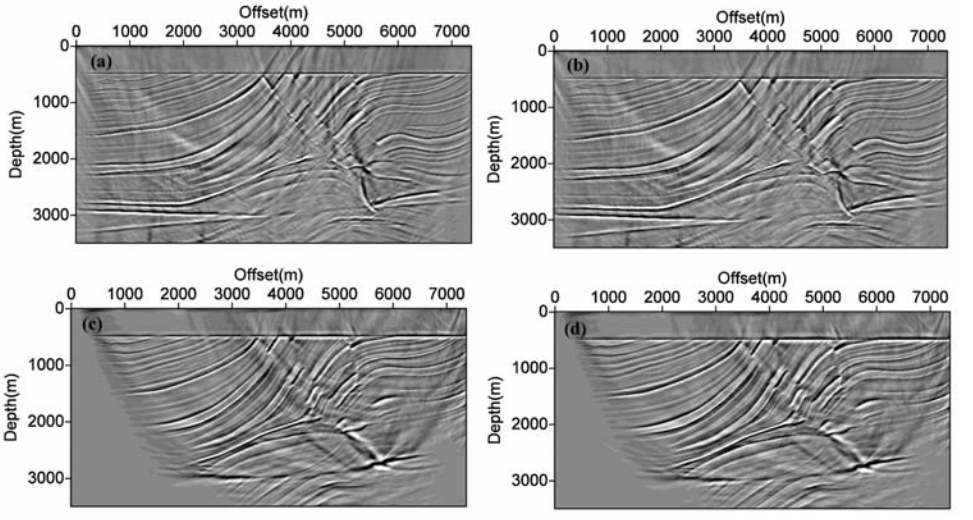

Fig. 7. Image of PLSRTM with static encoding (single plane-wave) after 40 iterations (a) p = 0.0 ms/m; (c) p = 0.5 ms/m. Image of PLSRTM with static encoding (single plane-wave) after 80 iterations (b) p = 0.0 ms/m; (d) p = 0.5 ms/m.

In order to further suppress the migration artefacts and improve imaging quality, all 24 plane-wave records are processed by prestack PLSRTM with static encoding. The stacked images of 24 plane-waves are shown in Fig. 8, in which the artefacts are completely suppressed and all structures are well imaged with high resolution and balanced amplitude.

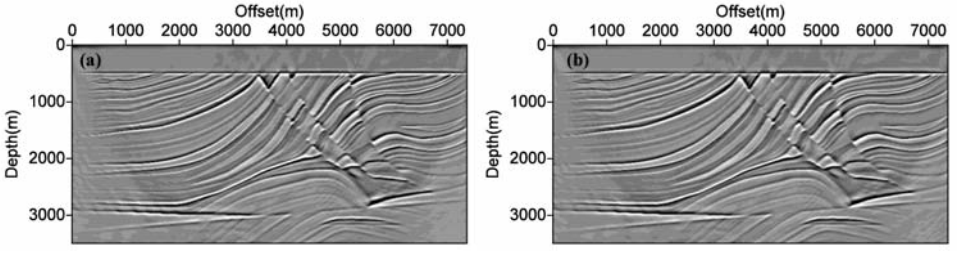

Fig. 8. Stacked image of PLSRTM with static encoding (24 plane-wave) after (a) 40 iterations; (b) 80 iterations.

Improved encoding strategies

From the synthetic test, we know that prestack PLSRTM has the advantages of well migration artefacts suppression and high imaging quality. But its computation is np times (np is the number of computed plane-waves) compared with PLSRTM of single plane-wave. In order to obtain a high quality image with less computation, PLSRTM is implemented with dynamic encoding and hybrid encoding strategies, where the ray parameters of encoded plane-waves range from -0.2 to $+0.2$ ms/m (corresponding to the angle ranging from -30 to $+30$ degrees). Fig. 9 shows the PLSRTM images with dynamic encoding and hybrid encoding after 40 and 80 iterations, respectively. After 40 iterations, the images of dynamic encoding have better migration artefacts reduction than that of hybrid encoding. And both of the two strategies

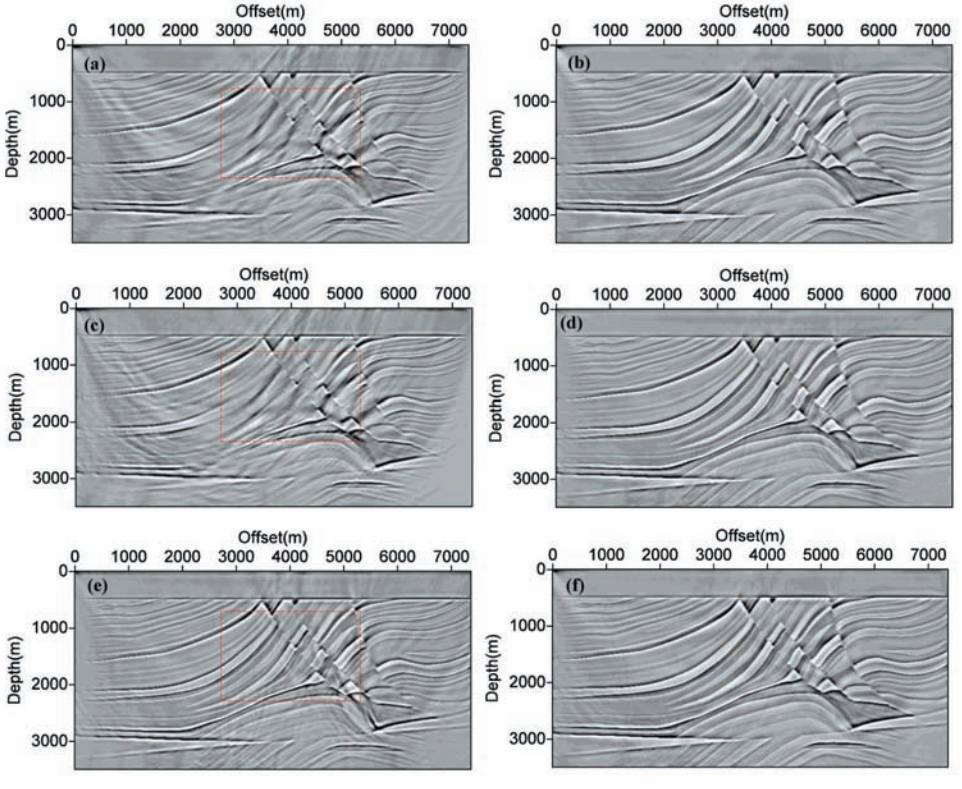

Fig. 9. Image of PLSRTM with dynamic encoding after (a) 40 iterations; (b) 80 iterations. Image of PLSRTM with hybrid encoding after (c) 40 iterations; (d) 80 iterations. Image of PLSRTM with random dynamic encoding after (e) 40 iterations; (f) 80 iterations.

produce blurry images of structures shown in red dashed boxes, because the inversion is lack of information from some specific shooting angles. When the inversion is finished after 80 iterations, the SNR and the resolution of the images with these two strategies are almost the same, but the I/O cost of hybrid encoding is only 0.2 times of the dynamic encoding.

In addition, we also introduce the randomized sampling approach to the dynamic encoding strategy in which one plane-wave is randomly chosen to compute the gradient at each iteration. PLSRTM images with random dynamic encoding after 40 and 80 iterations are showed in Figs. 9e and 9f, respectively. Compared with the images of PLSRTM with dynamic encoding and hybrid encoding after 40 iterations, image of PLSRTM with random dynamic encoding contains less artefacts, and the image in red dashed boxes is deblurred. From Fig. 9 we can know that: (1) PLSRTM with three encoding strategies can produce comparable images with less computation than prestack PLSRTM; (2) random dynamic encoding can suppress the migration artefacts and image all the

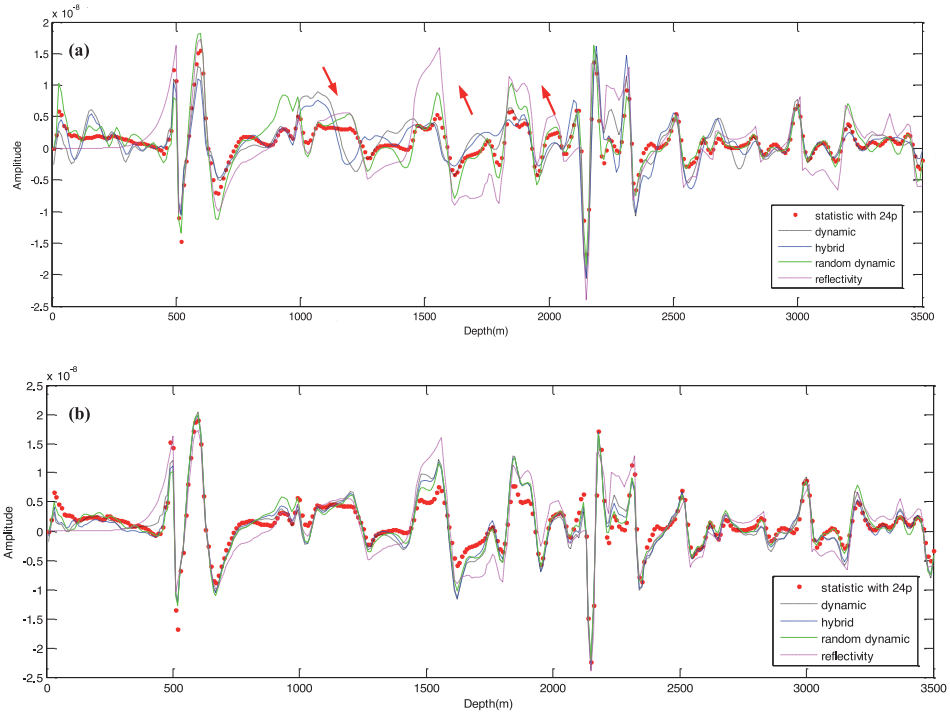

Fig. 10. Amplitude comparison of single trace (a) 40 iterations; (b) 80 iterations.

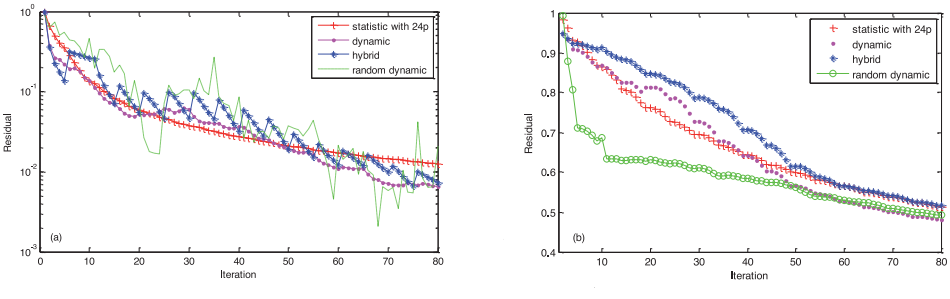

Fig. 11. Comparison of convergence curve with different encoding strategies (a) misfit residual; (b) model residual.

Numerically, the formula

$$\mathbf{SNR} = \left\| \mathbf{m}_{lsm}^{(k)} \right\| / \left\| \mathbf{m}_{lsm}^{(k)} - \mathbf{m}^{(k)} \right\| \quad , \tag{14}$$

is introduced to calculate the normalized SNR of PLSRTM with different encoding strategies, where $\mathbf{m}_{lsm}^{(k)}$ is the image of conventional LSRTM after k iterations. Fig. 12 shows the normalized SNR versus iteration number curve, in which PLSRTM with random dynamic encoding has much higher normalized SNR than other encoding strategies. The denominator of normalized SNR refers to not only migration artefacts but also model residual at the first few iterations because of the illumination difference between plane-waves with specific shooting angle and shot data. In some ways, the improvement at the first few iterations may partly owe to better illumination of randomized sampling approach. As iteration increases, the illumination difference becomes smoother and the improvement of normalized SNR becomes more convincing.

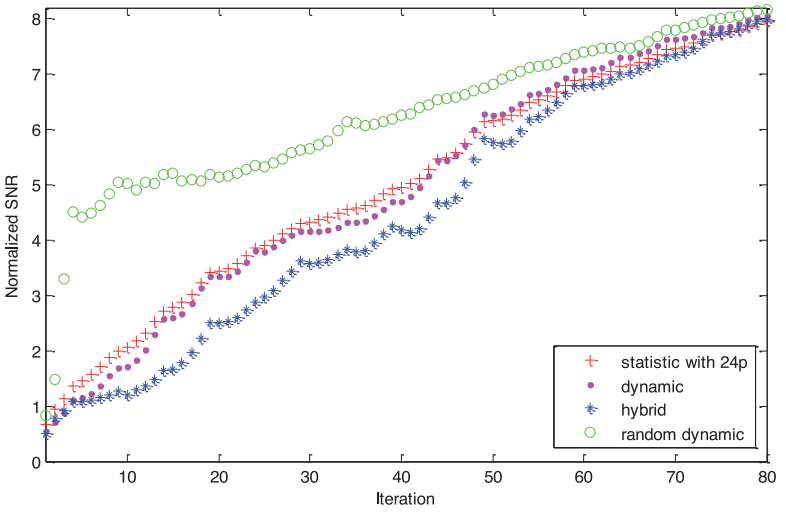

Fig. 12. Comparison of normalized SNR curve with different encoding strategies.

Under the inversion framework, the computational cost of PLSRTM to single plane-wave is about twice of the RTM to single shot in one iteration. Assuming the computation and I/O consumption of RTM is 1, the computational cost for PLSRTM equals to np × niter × 2/ns (the number of shots), I/O consumption equals to np/ns. The comparison of PLSRTM with different encoding strategies are summarized in Table 1 which shows that: PLSRTM with different encoding strategies can produce much better image with less computation compared with traditional RTM. In detail, PLSRTM with static encoding (single plane-wave) produces coarse images with moderate artefacts

and uneven illumination. But high-quality images can be obtained by stacking images corresponding to several plane-waves with the prestack approach with much more computation. Fortunately, the improved encoding strategies can help PLSRTM to producing high quality images with less computation. Among them, PLSRTM with hybrid encoding has the advantage of less I/O cost while PLSRTM with random dynamic encoding has the advantage of better migration artefacts suppression and illumination at original iterations.

Table 1. Comparison of PLSRTM with different encoding strategies for the synthetic data of Marmousi model.

	RTM	Static encoding (Single plane-wave)	Static encoding (24 plane-waves)	Dynamic encoding	Hybrid encoding	Random dynamic encoding
Computation	1	0.064	1.52	0.064	0.064	0.064
I/O cost	1	0.0013	0.032	0.106	0.021	0.106
Imaging quality	Good	Good	Best	Better	Better	Best
SNR	Lower	Lowest	Higher	Higher	High	Higher

Field data example

In this section, the PLSRTM with different encoding strategies are tested on a 2D field data set. The data is extracted from a 3D data set and there are 84 shots with a 90 m shot interval and each shot is recorded with 154 receivers with a 20 m interval. Firstly, the common shot data are transformed into common receiver gathers and then encoded to produce 16 plane-waves with ray parameters ranging from -0.3 ms/m to $+0.3$ ms/m.

Fig. 13 shows the imaging results of the RTM, and PLSRTM with different encoding strategies. From Fig. 13 we can see that PLSRTM with different encoding strategies produce improved images compared with conventional RTM. The final images of PLSRTM with different encoding strategies have comparable SNR and quality, but prestack PLSRTM with static encoding produces the image of highest SNR. Specifically, we exhibit the images of PLSRTM with dynamic encoding after 25 iterations (Fig. 14a), in which the energy of the steep structure in the deep part cannot be recovered. But this steep structure is well illuminated in the images of PSLRTM with random dynamic encoding (Fig. 14b). Then, the misfit convergence curve of PLSRTM with different encoding strategies is plotted in Fig. 15. When the velocity is not completely accurate, the convergences of PLSRTM with different encoding strategies are robust. And, the convergences of the prestack approach are the best, because the prestack image ensemble accommodates more unknowns to allow for better fitting of the observed data (Dai et al., 2013).

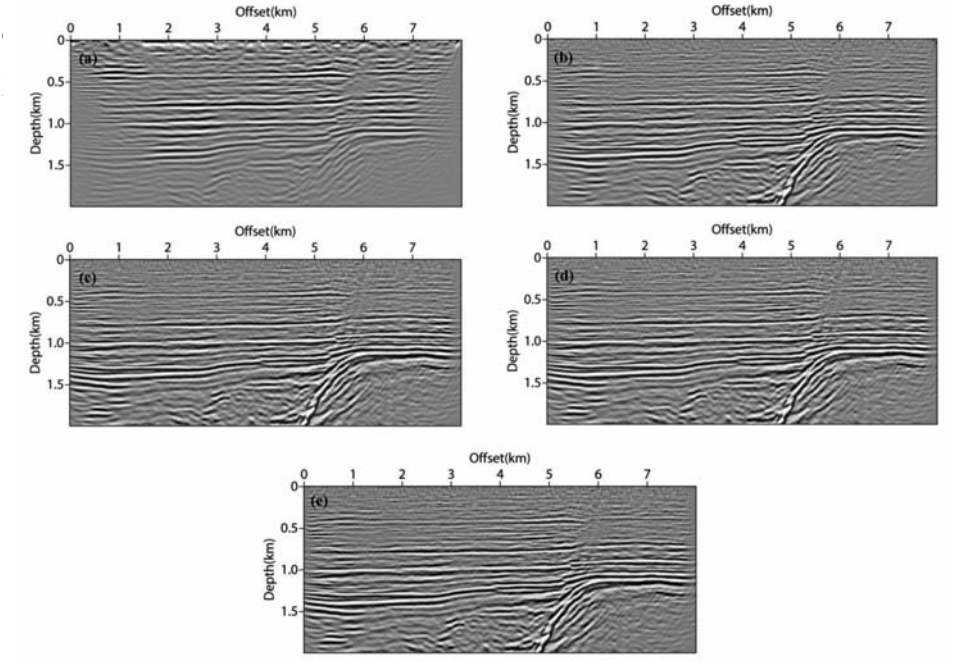

Fig. 13. Final images of RTM(a), PLSRTM with static encoding(b), dynamic encoding(c), hybrid encoding (d) and random dynamic encoding (e) strategies. Image of RTM lacks precision to illuminate all the structures.

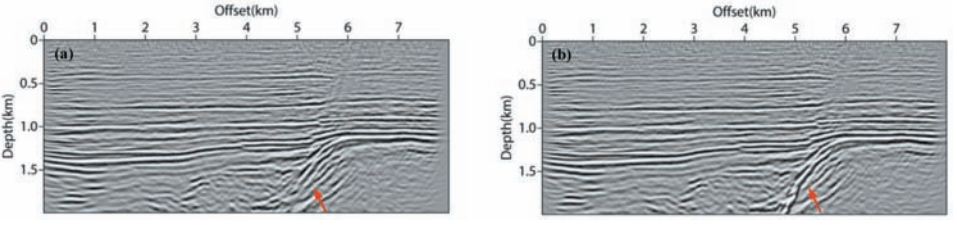

Fig. 14. Image of PLSRTM with dynamic encoding (a) and random dynamic encoding (b) after 25 iterations.

At last, the summary of this test is shown in Table 2. And # in Table 2 means that the imaging quality of PLSRTM with random dynamic encoding is even better than the dynamic and hybrid approaches. What we should point out here is that RTM and PLSRTM have different migration apertures. The migration aperture in the shot-profile migration is normally not the whole survey size while the migration aperture of PLSRTM needs to cover the whole survey. So this point is taken into account when we make the computational comparison between conventional RTM and PLSRTM. From Table 2 we can see that PLSRTM with improved encoding strategies can produce much better results with only 3.17 times of computation compared with conventional RTM. In terms of I/O cost, the hybrid approach is the most practical which need the minimum amount of memory if the input data is enormous.

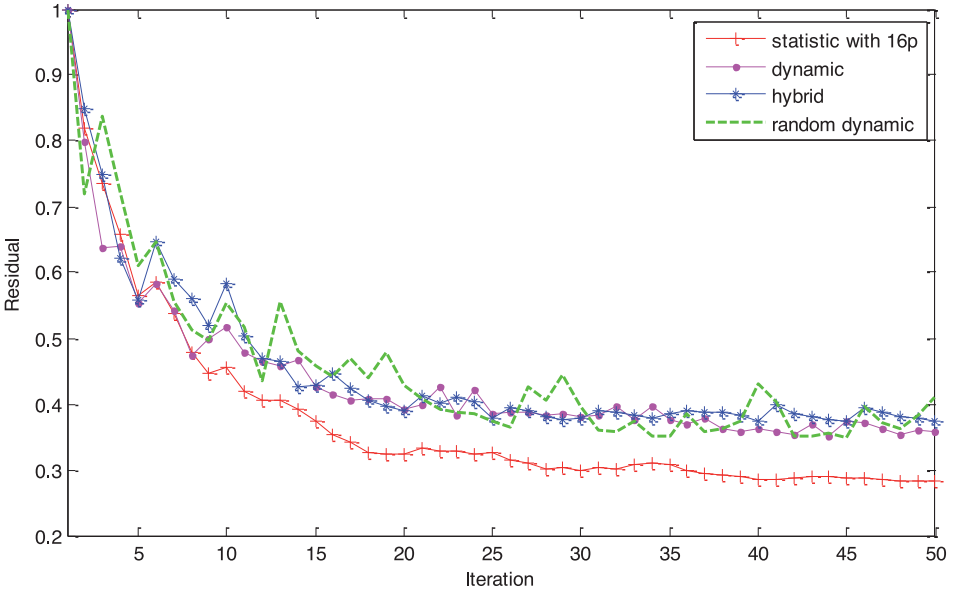

Fig. 15. The misfit convergence curve of PLSRTM with different encoding strategies.

Table 2. Comparison of PLSRTM with different encoding strategies for the field data.

	RTM	Static encoding (16 plane-waves)	Dynamic encoding	Hybrid encoding	Random dynamic encoding
Computation	1	29.7	3.17	3.17	3.17
I/O cost	1	0.5	1.59	0.32	1.59
Imaging quality	Good	Best	Better	Better	Better#

CONCLUSION

This paper presents the theory of PLSRTM with different encoding strategies. The hybrid encoding and random dynamic encoding approach are introduced to improve the convergence and efficiency of PLSRTM. To make a comprehensive comparison of different encoding strategies, the imaging tests are implemented with the synthetic data of Marmousi model and the 2D field data. With the imaging results, we can draw the following conclusions: (1) PLSRTM can suppress the aliasing artefacts introduced by plane-wave migration, and has

higher imaging resolution and better amplitude preservation compared to the traditional RTM method; (2) The development of dynamic encoding, hybrid encoding and random dynamic encoding strategies can greatly enhance the computational efficiency while ensuring imaging quality; (3) Different encoding strategies have their own advantages and shortcomings. Generally speaking, prestack PLSRTM with static encoding is of highest imaging quality, but the computational costs are still too expensive if the input data is enormous. So it is more suitable for the precise imaging of small exploration areas with not too much input data. PLSRTM with other encoding strategies has improved computational efficiency, which is fit for the processing of mass data. But the I/O cost is another problem for mass data processing in the GPU implementation, which can be solved by hybrid encoding approach with similar imaging quality and efficiency. PLSRTM with random dynamic encoding produces well illuminated images with less iteration, so it will be a good choice if the feature of underground structures is complicated. Therefore, appropriate strategies should be selected according to imaging requirements and the characteristics of encoding strategies when dealing with the field seismic data.

Since the background velocity is invariable at each iterations, the PLSRTM does a linearized inversion which can produce high quality images if the migration velocity does not differ much with the background velocity. Therefore, PLSRTM is less sensitive to migration velocity than conventional RTM method. In addition, as defined in eq. (5), the reflectivity in this paper is velocity perturbation rather than the real reflectivity. Actually, the reflectivity is relative to the reflection angles in the AVO/AVA inversion. However, only when the reflection angles equals to 90 degrees, the velocity perturbation in this paper has a linear relationship with the reflectivity. To perform AVO/AVA with PLSRTM, the relationship between reflectivity and reflection angles should to be considered.

ACKNOWLEDGEMENT

This research is supported by the National Nature Science Foundation of China (Grant No. 41104069, 41274124), the National Basic Research Program of China (973 Program, grant No. 2014CB239006, 2011CB202402) and the Open Foundation of SINOPEC Key Laboratory of Geophysics (Grant No. 33550006-15-FW2099-0033).

Thanks to the reviewer for the helpful comments. We thank for the help and discussion with Wei Dai and Xin Wang.

REFERENCES

Baysal, E., Kosloff, D.D. and Sherwood, J.W.C., 1983. Reverse time migration. Geophysics, 48: 1514-1524.

Beydoun, W.B. and Mendes, M., 1989. Elastic ray-born l2-migration/inversion. Geophys. J. Internat., 97: 151-160.

Berkhout, A.J., 1992. Areal shot record technology. J. Seismic Explor., 1: 251-264.

Claerbout, J.F., 1992. Earth Soundings Analysis: Processing Versus Inversion. Blackwell Scientific Publications, Oxford.

Chen, K.J., 1985. Optimization Computing Methods. Xidian University Press, Xi'an (in Chinese).

Chen, S.C. and Cao, J.Z., 2002. Plane-wave migration. Progr. Explor. Geophys., 25(3): 37-41 (in Chinese).

Dai., W., Wang, X. and Schuster, G.T., 2011. Least-squares migration of multisource data with a deblurring filter. Geophysics, 76(5): R135-R146.

Dai, W., Fowler, P. and Schuster, G.T., 2012. Multi-source least-squares reverse time migration. Geophys. Prosp., 60: 681-695.

Dai, W. and Schuster, G.T., 2013. Plane-wave least-squares reverse-time migration. Geophysics, 78(4): 5165-5177.

Huang, J.P., Cao, X.L., Li, Z.C., Sun, Y.S., Li, C. and Gao, G.C., 2014. Application of least-square reverse time migration in the high resolution imaging of near-surface. Oil Geophys. Prosp., 49: 112 (in Chinese).

Jin, S., Madariaga, R., Virieux, J. and Lambaré, G., 1992. Two-dimensional asymptotic iterative elastic inversion. Geophys. J. Internat., 108: 575-588.

Lambaré, G., Virieux, J., Madariaga, R. and Jin, S., 1992. Iterative asymptotic inversion of seismic profiles in the acoustic approximation. Geophysics, 57: 1138-1154.

Li, C., Huang, J.P. and Li, Z.C., 2014a. Application of plane-wave least square migration in fault block reservoirs: a case study. Extended Abstr., 76th EAGE Conf., Amsterdam.

Li. C., Huang, J.P., Li, Z.C. and Li, Q.Y., 2014b. Plane-wave least square reverse time migration for rugged topography. Expanded Abstr., 84th Ann. Internat. SEG Mtg., Denver: 3742-3746.

Liu, F., Stolt, R.H., Hanson, D.W. and Day, R.S., 2002. Plane wave source composition: an accurate phase encoding scheme for prestack migration. Expanded Abstr., 72nd Ann. Internat. SEG Mtg., Salt Lake City.

Luo, Y. and Schuster, G.T., 1991. Wave-equation traveltime inversion. Geophysics, 56: 645-653.

Mosher, C.C., Foster, D.J. and Hassanzadeh, S., 1997. Common angle imaging with offset plane waves. Expanded Abstr., 67th Ann. Internat. SEG Mtg., Dallas: 1379-1382.

Nemeth, T., Wu, C. and Schuster, G.T., 1999. Least-squares migration of incomplete reflection data. Geophysics, 64: 208-221.

Schuster, G.T., Wang, X., Huang, Y., Dai, W. and Boonyasiriwat, C., 2011. Theory of multisource crosstalk reduction by phase-encoded statics. Geophys. J. Internat., 184: 1289-1303.

Tarantola, A., 1984. Inversion of seismic reflection data in the acoustic approximation. Geophysics, 49: 1259-1266.

Tarantola, A., 1987. Inverse Problem Theory: Methods for Data Fitting and Model Parameter Estimation. Elsevier Science Publishers, Amsterdam.

Wang, X., Huang, Y., Dai, W. and Schuster, G.T., 2014. 3D Plane-wave least-squares Kirchhoff migration. Expanded Abstr., 84th Ann. Internat SEG Mtg., Denver.

Zhang, Y., Sun, J., Notfors, C., Gray, S.H., Chernis, L. and Young, J., 2005. Delayed-shot 3D depth migration. Geophysics, 70(5): E21-E28.